

Terahertz-Band Channel and Beam Split Estimation via Array Perturbation Model

Ahmet M. Elbir, *Senior Member, IEEE*, Wei Shi, Anastasios K. Papazafeiropoulos, *Senior Member, IEEE*, Pandelis Kourtessis, and Symeon Chatzinotas, *Senior Member, IEEE*

Abstract—For the demonstration of ultra-wideband bandwidth and pencil-beamforming, the terahertz (THz)-band has been envisioned as one of the key enabling technologies for the sixth generation networks. However, the acquisition of the THz channel entails several unique challenges such as severe path loss and beam-split. Prior works usually employ ultra-massive arrays and additional hardware components comprised of time-delayers to compensate for these losses. In order to provide a cost-effective solution, this paper introduces a sparse-Bayesian-learning (SBL) technique for joint channel and beam-split estimation. Specifically, we first model the beam-split as an array perturbation inspired from array signal processing. Next, a low-complexity approach is developed by exploiting the line-of-sight-dominant feature of THz channel to reduce the computational complexity involved in the proposed SBL technique for channel estimation (SBCE). Additionally, based on federated-learning, we implement a model-free technique to the proposed model-based SBCE solution. Further to that, we examine the near-field considerations of THz channel, and introduce the range-dependent near-field beam-split. The theoretical performance bounds, i.e., Cramér-Rao lower bounds, are derived for near- and far-field parameters, e.g., user directions, ranges and beam-split, and several numerical experiments are conducted. Numerical simulations demonstrate that SBCE outperforms the existing approaches and exhibits lower hardware cost.

Index Terms—Terahertz, channel estimation, beam split, sparse Bayesian learning, near-field, federated learning.

I. INTRODUCTION

Looking to 2030 and beyond, the sixth generation (6G) wireless networks require a revolutionary enhancement on data transmission ($> 100\text{Gb/s}$), extremely lower latency ($< 1\text{ms}$) and ultra reliability (99.999%) [1]. In order to meet these demands, the use of terahertz (THz) band frequencies has been envisioned as a promising solution exhibiting ultra-wideband bandwidth and enhanced pencil beamforming [2, 3].

This work has been submitted to the IEEE for publication. Copyright may be transferred without notice, after which this version may no longer be accessible.

This work was supported in part by the Natural Sciences and Engineering Research Council of Canada (NSERC), Ericsson Canada, and the ERC Project AGNOSTIC.

A. M. Elbir is with Interdisciplinary Centre for Security, Reliability and Trust (SnT) at the University of Luxembourg, Luxembourg (e-mail: ahmetmelbir@gmail.com).

W. Shi is with the School of Information Technology, Carleton University, Ottawa, Canada (e-mail: wei.shi@carleton.ca).

A. K. Papazafeiropoulos is with the CIS Research Group, University of Hertfordshire, Hatfield, U. K., and SnT at the University of Luxembourg, Luxembourg (e-mail: tapapazaf@gmail.com).

P. Kourtessis is with the CIS Research Group, University of Hertfordshire, Hatfield, U. K. (e-mail: p.kourtessis@herts.ac.uk).

S. Chatzinotas is with the SnT at the University of Luxembourg, Luxembourg (e-mail: symeon.chatzinotas@uni.lu).

The definition of the THz band varies among different IEEE communities. While IEEE Terahertz Technology and Applications Committee focus on $0.3 - 3$ THz, the IEEE Transactions on Terahertz Science and Technology Journal targets $0.3 - 10$ THz [4, 5]. On the other hand, recent works on wireless communications usually define this band as $0.1 - 10$ THz with a large overlap with millimeter-wave (mm-Wave) frequencies (e.g., $0.03 - 0.3$ THz) [4].

Compared to its mm-Wave counterpart, the THz-band channel exhibits several THz-specific challenges that should be taken into account. These unique THz features, among others, include high path loss due to spreading loss and molecular absorption, shorter transmission range, distance-dependent bandwidth and beam-split (see, e.g., Fig. 1) [2, 4, 6]. Furthermore, the THz channels are extremely sparse and modeled as line-of-sight (LoS)-dominant and non-LoS (NLoS)-assisted models [4, 7–12]. On the other hand, both LoS and NLoS paths are significant in the mm-Wave channel [13]. In order to compensate the severe path loss, analogous to massive multiple-input multiple-output (MIMO) array in mm-Wave design, ultra-massive (UM) MIMO array configurations are proposed [5, 14]. The UM-MIMO design comprises huge number of antennas which are densely-positioned (e.g., $5 \times 5 \text{ cm}^2$) due to extremely small wavelength [6]. As a result, the usage of dedicated radio-frequency (RF) chain for each antenna element involves extreme hardware cost and labor. The hybrid design configurations, i.e., joint usage of analog and digital beamformers seems to be major possible solution as it was first envisioned for mm-Wave massive MIMO systems in 5G [15–18]. In order to exploit low cost system design, the hybrid architecture involve small (large) number of digital (analog) beamformers. Although the digital beamformers are subcarrier-dependent, the analog phase shifters are designed as subcarrier-independent components. This causes *beam-split* phenomenon, i.e., the generated beams at different subcarriers split into different directions (see, e.g., Fig. 1) because of ultra-wide bandwidth and large number of antennas [8, 19, 20]. In mm-Wave, at which the subcarrier frequencies are relatively closer than THz, *beam-squint* is broadly used to describe the same phenomenon [13, 21, 22]. The beam-split affects the system performance and causes severe degradations in terms of spectral efficiency, normalized mean-squared-error (NMSE) and bit-error-rate (BER). For instance, the beam-split is approximately 4° (0.4°) for 0.3 THz with 30 GHz (60 GHz with 1 GHz) bandwidth, respectively for a broadside user (see Fig. 1) [6].

With the aforementioned THz-specific features, THz chan-

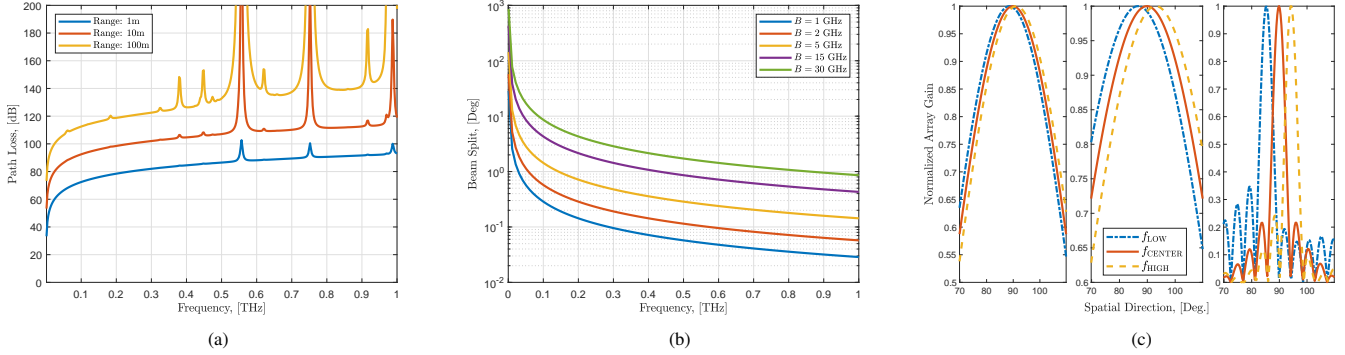


Fig. 1. THz-band characteristics: (a) path loss (in dB) due to molecular absorption for various transmission ranges, (b) beam-split (in degrees) in different bandwidths for a broadside user, and (c) normalized array gain with respect to spatial direction at low, center and high end subcarriers for (Left) 3.5 GHz, $B = 0.1$ GHz; (Middle) 28 GHz, $B = 2$ GHz; and (Right) 300 GHz, 30 GHz, respectively.

nel estimation is regarded as an even more challenging problem than that of mm-Wave. In prior studies, THz channel estimation has been investigated in [19, 23–31]. However, most of these works either ignore the effect of beam-split [23–26, 32] or consider only the narrowband case [27–29], without exploiting the ultra-wide bandwidth property, the key reason of climbing to THz-band. Further to that, [33] proposed a machine learning (ML)-based SBL approach for wideband THz channel estimation by aiming at mitigating the effect of beam-split via refining the angular grid resolution. However, no performance improvement was observed in terms of NMSE by enhancing the grid resolution. In fact, the beam-split compensation requires certain signal processing or hardware techniques to be handled properly.

Despite the prominence of THz channel estimation, there are only a few recent works in the literature on mitigating the beam-split effect. The existing solutions are categorized into two classes, i.e., hardware-based techniques [30] and algorithmic methods [19, 31]. The first category of solutions consider employing time delay (TD) networks together with phase shifters to realize virtual subcarrier-dependent analog beamformers to mitigate beam-split. In particular, [30] devises a generalized simultaneous orthogonal matching pursuit (GSOMP) technique by exploiting the subcarrier-dependent information collected via TD network hence achieves close to minimum MSE (MSE) performance. However, these solutions require additional hardware, i.e., each phase shifter is connected to multiple TDs, each of which consumes approximately 100 mW, which is more than that of a phase shifter (40 mW) in THz [6]. The second category of solutions do not employ additional hardware components. Instead, advanced signal processing techniques have been proposed to compensate beam-split. Specifically, an OMP-based beam-split pattern detection (BSPD) approach was proposed in [19] to recover the beam-support pattern among subcarriers and construct one-to-one match between the physical and spatial (i.e., deviated due to beam-split in the beamspace) directions. In [31], a beamspace support alignment (BSA) technique was introduced to align the deviated spatial beam directions among the subcarriers. Although both BSPD and BSA are based on OMP, the latter exhibits lower NMSE for THz channel

estimation. Nevertheless, both methods suffer from inaccurate support detection and low precision for estimating the physical channel directions.

Due to short transmission range in THz, near-field spherical-wave models are considered for THz applications [6, 34]. In particular, in the far-field the transmitted signal reaches to the users as plane-wave whereas the plane wavefront is spherical in the near-field when the transmission range is shorter than the Rayleigh distance. Thus, the near-field effects should be taken into account for accurate channel modeling. In [34], THz near-field beamforming problem has been considered and TD network-based approach was proposed while the THz channel was assumed to be known *a priori*.

In this paper, THz channel estimation in the presence of beam-split is examined. By exploiting the extreme sparsity of THz channel, we first approach the problem from the sparse recovery optimization perspective. Then, we introduce a novel approach to model the beam-split as an array perturbation as inspired by the array imperfection models, e.g., mutual coupling, gain-phase mismatch, in array signal processing context [35–37]. The array perturbation model allows us to establish a linear transformation between the nominal (constructed via physical directions) and actual (beam-split corrupted) steering vectors. Next, we propose a sparse Bayesian learning (SBL) approach to jointly estimate both THz channel and beam-split. The SBL method has been shown to be effective for sparse signal reconstruction from underdetermined observations [38–40]. Compared to other existing signal estimation techniques, e.g., multiple signal classification (MUSIC) [41] and the ℓ_p -norm ($0 \leq p \leq 1$) techniques such as compressed sensing (CS) [42], SBL outperforms these techniques in terms of precision and convergence [43]. Although SBL has been widely used for both channel estimation [37] and direction-of-arrival (DoA) estimation [36, 44], the proposed SBL-based channel estimation (SBCE) approach differentiates from these studies by jointly estimating multiple hyperparameters, e.g., physical channel directions and beam-split as well as array perturbation-based beam-split model. The proposed approach is advantageous in terms of complexity since it does not require any additional hardware components as in TD-based works, and it exhibits close to optimum performance

for both THz channel and beam-split estimation. Furthermore, the estimation of beam-split allows one to design the hybrid beamformers in massive/UM MIMO systems with more accuracy in a simpler way. The main contributions of this work are summarized as follows:

- 1) We propose a novel approach to model beam-split as an array perturbation, and design a transformation matrix between the nominal and actual steering vectors in order to accurately estimate both THz channel and beam-split.
- 2) An SBL approach is devised to jointly estimate the physical channel directions and beam-split. In order to reduce the computational complexity involved in SBL iterations, we exploit the LoS-dominant feature of THz channel and design the array perturbation matrix based on a single unknown parameter, i.e., the beam-split. Thus, instead of designing the array perturbations via a full matrix with distinct elements, we consider a diagonal structure, that can be easily represented via only beam-split knowledge.
- 3) We also propose a model-free approach based on federated learning (FL) to ease the communication overhead while maintaining satisfactory NMSE performance. Different from our preliminary work in [31], we consider SBCE method for data labeling, hence it is called sparse Bayesian FL (SBFL).
- 4) We investigate the near-field considerations for THz transmission, and derive the near-field beam-split, which is both range- and direction-dependent.
- 5) In addition, the theoretical performance bounds for both physical channel directions and beam-split estimation are examined and the corresponding Cramér-Rao lower bounds (CRBs) have been derived.

Paper Organization: The rest of the paper is organized as follows. In Sec. II, we present the array signal model and formulate the THz channel estimation problem. Next, our proposed SBCE approach is introduced in Sec. III. The near-field model for beam-split and the proposed SBFL approach are given in Sec. IV and Sec. V, respectively. We present extensive numerical simulations in Sec. VI, and finalize the paper with conclusions in Sec. VII.

Notation: Throughout the paper, $(\cdot)^\top$ and $(\cdot)^\mathsf{H}$ denote the transpose and conjugate transpose operations, respectively. For a matrix \mathbf{A} ; $[\mathbf{A}]_{ij}$ and $[\mathbf{A}]_k$ correspond to the (i, j) th entry and k th column while \mathbf{A}^\dagger denotes the Moore-Penrose pseudo-inverse of \mathbf{A} . A unit matrix of size N is represented by \mathbf{I}_N , ∇ represents the gradient operation, and $\text{Tr}\{\cdot\}$ stands for the trace operation. $\|\cdot\|_0$, $\|\cdot\|_1$, $\|\cdot\|_2$ and $\|\cdot\|_{\mathcal{F}}$ denote the ℓ_0 , ℓ_1 , ℓ_2 and Frobenius norms, respectively.

II. SIGNAL MODEL AND PROBLEM FORMULATION

We consider a multi-user wideband UM-MIMO-OFDM (orthogonal frequency division multiplexing) architecture with M subcarriers, wherein the base station (BS) is equipped with N_T antennas and N_{RF} radio-frequency (RF) chains to serve K single-antenna users. In the downlink, the BS first precodes the data symbols $\mathbf{s}[m] = [s_1[m], \dots, s_K[m]]^\top$ ($m \in \mathcal{M} = \{1, \dots, M\}$) via the subcarrier-dependent

baseband beamformer $\mathbf{F}_{\text{BB}}[m] \in \mathbb{C}^{K \times K}$. Then, the resulting signal $\mathbf{F}_{\text{BB}}[m]\mathbf{s}[m] \in \mathbb{C}^K$ is transformed to the time domain via an M -point inverse discrete Fourier transform (IDFT). After adding cyclic prefix (CP), the BS employs subcarrier-independent analog beamformers $\mathbf{F}_{\text{RF}} \in \mathbb{C}^{N_T \times N_{\text{RF}}}$ ($N_{\text{RF}} = K < N_T$). The analog beamformers, which are realized with phase shifters are used to steer the generated beams toward users, hence they have constant-modulus constraint, i.e., $|\mathbf{F}_{\text{RF}}|_{i,j} = \frac{1}{\sqrt{N_T}}$ as $i = 1, \dots, N_{\text{RF}}$ and $j = 1, \dots, N_T$. Additionally, we have the power constraint $\sum_{m=1}^M \|\mathbf{F}_{\text{RF}}\mathbf{F}_{\text{BB}}[m]\|_{\mathcal{F}}^2 = MK$ that is enforced by the normalization of the baseband beamformers $\{\mathbf{F}_{\text{BB}}[m]\}_{m \in \mathcal{M}}$. Let us define the transmitted signal as

$$\mathbf{z}[m] = \mathbf{F}_{\text{RF}}\mathbf{F}_{\text{BB}}[m]\mathbf{s}[m]. \quad (1)$$

Then, the received signal at the k th user in the m th subcarrier is

$$y_k[m] = \mathbf{h}_k^\top[m]\mathbf{z}[m] + w_k[m], \quad (2)$$

where $w_k[m] \in \mathbb{C}$ denotes the additive white Gaussian noise (AWGN) vector with $w_k[m] \sim \mathcal{CN}(0, \mu^2)$.

A. THz Channel Model

In THz transmission, the wireless channel can be modeled by the superposition of a single LoS path and the contribution of a few NLoS paths, which are weak due to large reflection losses, scattering and refraction [4, 7–9]. In recent works, measurement campaigns at 140 GHz have been reported [45, 46]. In particular, [46] states that, while the delay/angular spread at 140 GHz and lower frequencies are comparable, the correlation distance of shadow fading at the former is much shorter. While the ray-tracing techniques assume the channel to be sparse and dominated by the LoS component for the graphene nano-transceivers [4], the other channel models such as the 3GPP model [47, 48] are also popular for THz transmission.

Let $p(\tau)$ denote a pulse shaping function for T_s -space signaling evaluated at τ seconds. Then, the THz delay- d UM-MIMO channel in time domain is given by

$$\bar{\mathbf{h}}_k(d) = \sqrt{\frac{N_T}{L}} p(dT_s - \tau_{k,l}) \left(\underbrace{\alpha_k^{m,1} \mathbf{a}'(\theta_{k,m,1})}_{\text{LoS}} + \underbrace{\sum_{l=2}^L \alpha_k^{m,l} \mathbf{a}'(\theta_{k,m,l})}_{\text{NLoS}} \right), \quad (3)$$

where $\alpha_k^{m,l} \in \mathbb{C}$ is the complex path gain. L is the total number of paths and $\tau_{k,l}$ is the time delay of the l th path, for which $l = 1$ corresponds to the LoS path. After performing M -point DFT of the delay- d channel in (3) as $\mathbf{h}_k[m] = \sum_{d=0}^{D-1} \bar{\mathbf{h}}_k(d) e^{-j \frac{2\pi m}{M} d}$ for CP length $D \leq M$ [23,

49]. Then, the channel vector of the k th user at the m th subcarrier becomes

$$\mathbf{h}_k[m] = \sqrt{\frac{N_T}{L}} \left(\underbrace{\alpha_k^{m,1} \mathbf{a}'(\theta_{k,m,1})}_{\text{LoS}} + \underbrace{\sum_{l=2}^L \alpha_k^{m,l} \mathbf{a}'(\theta_{k,m,l})}_{\text{NLoS}} \right) e^{-j2\pi\tau_{k,l}f_m}, \quad (4)$$

where $f_m = f_c + \frac{B}{M}(m-1 - \frac{M-1}{2})$ is the m th subcarrier frequency with f_c and B being the carrier frequency and the bandwidth, respectively. $\theta_{k,m,l}$ denote the subcarrier-dependent spatial channel directions as

$$\theta_{k,m,l} = \frac{2f_m}{c_0} \bar{d} \vartheta_{k,l} = \frac{f_m}{f_c} \vartheta_{k,l}, \quad (5)$$

with $\vartheta_{k,l} = \sin \tilde{\vartheta}_{k,l}$ being the physical direction for the l -th path with $\tilde{\vartheta}_{k,l} \in [-\frac{\pi}{2}, \frac{\pi}{2}]$. In (5), c_0 is speed of light, and $\bar{d} = \frac{c_0}{2f_c}$ is the half-wavelength antenna spacing. $\mathbf{a}'(\theta_{k,m,l}) \in \mathbb{C}^{N_T}$ is the steering vector¹ corresponding to $\theta_{k,m,l}$ and defined for a uniform linear array (ULA)² as

$$\mathbf{a}'(\theta_{k,m,l}) = \frac{1}{\sqrt{N_T}} [1, e^{j\pi\theta_{k,m,l}}, \dots, e^{j\pi(N_T-1)\theta_{k,m,l}}]^\top. \quad (6)$$

The channel vector in (4) can also be expressed in a compact form as

$$\mathbf{h}_k[m] = \mathbf{A}'_k[m] \tilde{\mathbf{x}}_k[m], \quad (7)$$

where $\mathbf{A}'_k[m] = [\mathbf{a}'(\theta_{k,m,1}), \dots, \mathbf{a}'(\theta_{k,m,L})] \in \mathbb{C}^{N_T \times L}$ and $\tilde{\mathbf{x}}_k[m] = [\alpha_k^{m,1} e^{-j2\pi\tau_{k,1}f_m}, \dots, \alpha_k^{m,L} e^{-j2\pi\tau_{k,L}f_m}]^\top \in \mathbb{C}^L$.

Note that $\theta_{k,m,l} \approx \vartheta_{k,l}$ when $f_m \approx f_c$ (see, e.g., Fig. 1). This observation allows us to employ subcarrier-independent analog beamformers (i.e., \mathbf{F}_{RF}) for $m \in \mathcal{M}$ in conventional mm-Wave systems [13, 21, 22]. However, beam-split implies that with wider system bandwidth $|f_m - f_c|$, physical directions $\vartheta_{k,l}$ deviate from the spatial directions $\theta_{k,m,l}$. Hence, we define the beam-split as the difference between the spatial and physical directions as

$$\Delta_{k,l}[m] = \theta_{k,m,l} - \vartheta_{k,l} = \left(\frac{f_m}{f_c} - 1 \right) \vartheta_{k,l}, \quad (8)$$

which only depends on the frequency ratio $\frac{f_m}{f_c}$ and $\vartheta_{k,l}$.

B. Problem Formulation

In order to estimate the THz channel, the BS transmits known pilot signals which are received and processed simultaneously by all users during channel training [8, 19, 23]. Let $\tilde{\mathbf{S}}[m] = \text{diag}\{\tilde{s}_1[m], \dots, \tilde{s}_P[m]\} \in \mathbb{C}^{P \times P}$ be the set of pilots, where P is the number of pilot signals. We assume a block-fading channel, wherein the coherence time is longer than the training time [49]. Let us denote the resulting beamformer

¹We denote the nominal and actual steering vectors by $\mathbf{a}'(\theta)$ and $\mathbf{a}(\vartheta)$ for notational clarity. Please see (15) for the definition of $\mathbf{a}(\vartheta)$.

²Although ULA is considered in this work, the proposed approach can straightforwardly be extended for other array geometries, e.g., uniform rectangular array (URA), array-of-subarray (AoSA) [4, 14] or group-of-subarrays (GoSA) [5].

vector at the BS as $\tilde{\mathbf{f}}_p[m] \in \mathbb{C}^{N_T}$ for $p = 1, \dots, P$. Then, the k th user collects the $P \times 1$ received signals as

$$\bar{\mathbf{y}}_k[m] = \tilde{\mathbf{S}}[m] \bar{\mathbf{F}}[m] \mathbf{h}_k[m] + \mathbf{w}_k[m], \quad (9)$$

where $\bar{\mathbf{F}} = \tilde{\mathbf{F}}^\top \in \mathbb{C}^{P \times N_T}$ with $\tilde{\mathbf{F}} = [\tilde{\mathbf{f}}_1[m], \dots, \tilde{\mathbf{f}}_P[m]]$ being the beamformer matrix, $\bar{\mathbf{y}}_k[m] = [y_{k,1}[m], \dots, y_{k,P}[m]]^\top \in \mathbb{C}^P$ and $\mathbf{w}_k = [w_{k,1}[m], \dots, w_{k,P}[m]]^\top \in \mathbb{C}^P$. Without loss of generality, by assuming $\bar{\mathbf{F}}[m] = \bar{\mathbf{F}}$ and $\tilde{\mathbf{S}}[m] = \mathbf{I}_P$, (9) becomes

$$\bar{\mathbf{y}}_k[m] = \bar{\mathbf{F}} \mathbf{h}_k[m] + \mathbf{w}_k[m]. \quad (10)$$

Estimating the channel from (10) can be performed via the traditional least squares (LS) and MMSE techniques as

$$\begin{aligned} \mathbf{h}_k^{\text{LS}}[m] &= (\bar{\mathbf{F}}^\text{H} \bar{\mathbf{F}})^{-1} \bar{\mathbf{F}}^\text{H} \bar{\mathbf{y}}_k[m], \\ \mathbf{h}_k^{\text{MMSE}}[m] &= (\mathbf{R}_k^{-1}[m] + \bar{\mathbf{F}}^\text{H} \mathbf{R}_k^{-1}[m] \bar{\mathbf{F}})^{-1} \bar{\mathbf{F}}^\text{H} \bar{\mathbf{y}}_k[m], \end{aligned} \quad (11)$$

respectively, where $\mathbf{R}_k[m] = \mathbb{E}\{\mathbf{h}_k[m] \mathbf{h}_k^\text{H}[m]\}$ is the channel covariance matrix. The estimators in (11) require $P \geq N_T$, which entails high channel training overheads and time due to the UM number of antennas. Further to that, the effect of beam-split is not taken into account for the LS method which yields poor performance, and prior information on the channel covariance is needed in MMSE estimator.

Hence, our goal is to efficiently estimate the THz channel $\mathbf{h}_k[m]$ for $m \in \mathcal{M}$ in the presence of beam-split when the number of received pilot signals is small. To this end, we exploit the sparsity of the THz channel and introduce an SBL-based approach in the following.

III. SBL FOR THZ CHANNEL ESTIMATION

The SBL method has been shown to be effective for sparse signal reconstruction. In this section, we first present the sparse THz signal model and introduce the proposed array perturbation model and an efficient approach for joint THz channel and beam-split estimation.

A. Sparse THz Channel Model

Due to employing UM number of antennas to compensate the significant path loss in THz frequencies, the THz channel is *extremely-sparse* in the angular domain (i.e., $L \ll N_T$) [7, 14]. In order to exploit the sparsity of THz-band, the channel in (4) can be expressed as

$$\mathbf{h}_k[m] = \mathbf{F} \mathbf{x}_k[m], \quad (12)$$

where $\mathbf{x}_k[m] \in \mathbb{C}^N$ is an L -sparse vector, i.e., $\|\mathbf{x}_k[m]\|_0 = L$ and $\mathbf{F} = [\mathbf{a}(\phi_1), \dots, \mathbf{a}(\phi_N)] \in \mathbb{C}^{N_T \times N}$ denotes an over-complete dictionary matrix composed of the steering vector $\mathbf{a}(\phi_n) \in \mathbb{C}^{N_T}$ with $\phi_n = \frac{2n-1}{N}$ for $n = 1, \dots, N$. Hence, the resolution of \mathbf{F} is $\rho = 1/N$.

Next, we assume that the users collects only $P = N_{\text{RF}}$ pilot signals, where $L \leq P \ll N_T$. Further, we model the subcarrier-independent matrix representing the precoder at the BS as $\mathbf{B} \in \mathbb{C}^{P \times N_T}$ with $|\mathbf{B}|_{i,j} = \frac{1}{\sqrt{N_T}}$. Then, the received signal at the k th user can be given as the following underdetermined system, i.e.,

$$\mathbf{y}_k[m] = \mathbf{B} \mathbf{F} \mathbf{x}_k[m] + \mathbf{w}_k[m], \quad (13)$$

where $\mathbf{y}_k[m] \in \mathbb{C}^P$ is the observation vector. Exploiting the sparsity of $\mathbf{x}_k[m]$ in (13), we formulate the following ℓ_1 -norm sparse recovery (SR) problem

$$\begin{aligned}\hat{\mathbf{x}}_k[m] &= \arg \min_{\mathbf{x}_k[m]} \|\mathbf{x}_k[m]\|_1 \\ \text{subject to: } &\|\mathbf{y}_k[m] - \mathbf{B}\mathbf{F}\mathbf{x}_k[m]\|_2^2 \leq \epsilon,\end{aligned}\quad (14)$$

where the residual ϵ is bounded with $\epsilon \leq \mu\sqrt{P + \kappa\sqrt{2P}}$, where κ is an adjustable parameter controlling the noise power $\mathbb{E}\{\|\mathbf{w}_k[m]\|_2^2\}$ [35, 42]. Using $\hat{\mathbf{x}}_k[m]$, the channel is estimated as $\hat{\mathbf{h}}_k^{\text{SR}}[m] = \mathbf{F}\hat{\mathbf{x}}_k[m]$.

B. Array Perturbation Based Beam-Split Model

In order to accurately mitigate the beam-split, we approach the problem from an array calibration point of view, wherein the beam-split is modeled as an array perturbation, e.g., mutual coupling, gain/phase mismatch [35–37]. Let us begin by rewriting the channel model in (4) as

$$\begin{aligned}\mathbf{h}_k[m] &= \sqrt{\frac{N_T}{L}} \sum_{l=1}^L \alpha_k^{m,l} \mathbf{U}_k[m] \mathbf{a}(\vartheta_{k,l}) e^{-j2\pi\tau_{k,l}f_m}, \\ &= \mathbf{U}_k[m] \mathbf{A}_k[m] \tilde{\mathbf{x}}_k[m],\end{aligned}\quad (15)$$

where $\mathbf{A}_k[m] = [\mathbf{a}(\vartheta_{k,1}), \dots, \mathbf{a}(\vartheta_{k,L})] \in \mathbb{C}^{N_T \times L}$ and $\mathbf{a}(\vartheta_{k,l}) \in \mathbb{C}^{N_T}$ denotes the array steering vector corresponding to the physical directions $\vartheta_{k,l}$. $\mathbf{U}_k[m] \in \mathbb{C}^{N_T \times N_T}$ denotes the array perturbation matrix which maps the nominal array steering matrix, i.e., $\mathbf{A}_k[m]$ to $\mathbf{A}'_k[m]$ which is perturbed due to beam-split. Hence, $\mathbf{U}_k[m]$ provides a linear transformation between the steering matrices corresponding to physical and spatial directions as

$$\mathbf{A}'_k[m] = \mathbf{U}_k[m] \mathbf{A}_k[m]. \quad (16)$$

Now, our aim is to rewrite the received signal $\mathbf{y}_k[m]$ as the linear combination of receiver output corresponding to the physical channel directions and some perturbation term. Hence, using (16) and (7), we get

$$\begin{aligned}\mathbf{y}_k[m] &= \mathbf{B}\mathbf{A}'_k[m]\tilde{\mathbf{x}}_k[m] + \mathbf{w}_k[m] \\ &= \mathbf{B}\mathbf{U}_k[m]\mathbf{A}[m]\tilde{\mathbf{x}}_k[m] + \mathbf{w}_k[m] \\ &= \mathbf{B}(\mathbf{A}[m]\tilde{\mathbf{x}}_k[m] + \bar{\mathbf{Q}}_k[m]\mathbf{u}_k[m]) + \mathbf{w}_k[m],\end{aligned}\quad (17)$$

where $\mathbf{u}_k[m] = \text{vec}\{\mathbf{U}_k[m]\} \in \mathbb{C}^{N_T^2}$, which includes the array perturbation terms in $\mathbf{U}_k[m]$. $\bar{\mathbf{Q}}_k[m]$ is an $N_T \times N_T^2$ matrix with the following structure, i.e.,

$$\bar{\mathbf{Q}}_k[m]\mathbf{u}_k[m] = (\mathbf{A}'_k[m] - \mathbf{A}_k[m])\tilde{\mathbf{x}}_k[m]. \quad (18)$$

Now, let us define $\tilde{\mathbf{P}}_k[m] = \mathbf{B}\mathbf{A}_k[m] \in \mathbb{C}^{P \times L}$ and $\tilde{\mathbf{Q}}_k[m] = \mathbf{B}\bar{\mathbf{Q}}_k[m] \in \mathbb{C}^{P \times N_T^2}$, then (17) becomes

$$\mathbf{y}_k[m] = \tilde{\mathbf{P}}_k[m]\tilde{\mathbf{x}}_k[m] + \tilde{\mathbf{Q}}_k[m]\mathbf{u}_k[m] + \mathbf{w}_k[m]. \quad (19)$$

The perturbed array formulation in (19) explicitly shows the relationship between the received signal $\mathbf{y}_k[m]$ and the perturbation parameters corresponding to the beam-split $\mathbf{u}_k[m]$. Hence, one can minimize the fitting error between $\mathbf{y}_k[m]$ and $\tilde{\mathbf{P}}_k[m]\tilde{\mathbf{x}}_k[m]$ to determine the physical channel directions as well as estimating the perturbation due to beam-split, as will be introduced in the following.

C. SBL

In the proposed SBL framework, we rewrite (19) in an overcomplete form. Hence, only in this part, we first drop the subscript $(\cdot)_k$ and $[m]$ for notational simplicity, and discuss the channel estimation stage for multi-user multi-subcarrier case later. Next, we use $\mathbf{Q} \in \mathbb{C}^{P \times N_T^2}$ instead of $\tilde{\mathbf{Q}}_k[m]$, and define $\mathbf{P} = \mathbf{B}\mathbf{F} \in \mathbb{C}^{P \times N}$ as the overcomplete version of $\tilde{\mathbf{P}}_k[m] \in \mathbb{C}^{P \times L}$ covering the whole angular domain with ϕ_n , $n = 1, \dots, N$. Also, we have $\mathbf{P}' = \mathbf{B}\mathbf{U}\mathbf{F} \in \mathbb{C}^{P \times N}$, i.e., the overcomplete version of the perturbed steering matrix $\mathbf{B}\mathbf{A}'_k[m] = \mathbf{B}\mathbf{U}_k[m]\mathbf{A}_k[m] \in \mathbb{C}^{P \times L}$. Then, (19) can be expressed as follows

$$\mathbf{y} = \mathbf{Px} + \mathbf{Qu} + \mathbf{w}, \quad (20)$$

where \mathbf{x} , \mathbf{u} and \mathbf{w} are $N \times 1$, $N_T^2 \times 1$ and $P \times 1$ vectors, respectively, as defined earlier with removed subscripts.

Now, we introduce a new set of variables $\boldsymbol{\sigma} = [\sigma_1, \dots, \sigma_N]^T$ as the variance of sparse vector $\mathbf{x} \sim \mathcal{CN}(\mathbf{0}, \boldsymbol{\Sigma})$, where $\boldsymbol{\Sigma} = \text{diag}\{\boldsymbol{\sigma}\}$. Then, we derive the statistical dependence of the received signal \mathbf{y} on the unknown parameters, i.e., the sparse vector \mathbf{x} , perturbation parameter \mathbf{u} , and the noise variance μ^2 . Toward this end, we look for the maximum likelihood estimate of these parameters to reconstruct the channel vector from the support of \mathbf{x} as $\hat{\mathbf{h}} = \hat{\mathbf{F}}\hat{\mathbf{x}}$.

The likelihood function of the received signal in (20) is

$$\begin{aligned}p(\mathbf{y}|\mathbf{x}; \mathbf{u}, \mu^2) &= \frac{1}{\pi\mu^2 N_T} \exp\left\{-\frac{1}{\mu^2} \|\mathbf{y} - \mathbf{P}'\mathbf{x}\|_2^2\right\} \\ &= \frac{1}{\pi\mu^2 N_T} \exp\left\{-\frac{1}{\mu^2} \|\mathbf{y} - \mathbf{Px} - \mathbf{Qu}\|_2^2\right\}.\end{aligned}\quad (21)$$

Now, we can use (21) to write the probability density function (pdf) of \mathbf{y} with respect to the hyperparameters $\boldsymbol{\sigma}$, \mathbf{u} and μ^2 as

$$\begin{aligned}p(\mathbf{y}; \boldsymbol{\sigma}, \mathbf{u}, \mu^2) &= \int p(\mathbf{y}|\mathbf{x}; \mathbf{u}, \mu^2) \times p(\mathbf{x}; \boldsymbol{\sigma}) d\mathbf{x} \\ &= \frac{1}{|\pi\boldsymbol{\Pi}_y|} \exp\left\{-\text{Tr}\{\boldsymbol{\Pi}_y^{-1}\mathbf{R}_y\}\right\},\end{aligned}\quad (22)$$

where $\boldsymbol{\Pi}_y \in \mathbb{C}^{P \times P}$ is the covariance of \mathbf{y} as

$$\boldsymbol{\Pi}_y = \mathbb{E}\{\mathbf{y}\mathbf{y}^H\} = \mathbf{P}'\boldsymbol{\Sigma}\mathbf{P}^H + \mu^2\mathbf{I}_P, \quad (23)$$

and $\mathbf{R}_y = \mathbf{y}\mathbf{y}^H \in \mathbb{C}^{P \times P}$.

Let us define the unknown parameters in a hyperparameter set $\mathcal{S} = \{\boldsymbol{\sigma}, \mathbf{u}, \mu^2\}$. Then, \mathcal{S} can be estimated by maximizing the pdf in (22), which is non-concave and computationally intractable due to the nonlinearities. Hence, we resort to the expectation-maximization (EM) algorithm, which iteratively converges to a local optimum [36–40]. Each EM iteration comprises two steps: E-step for *inference*, and M-step for *hyperparameter estimation* by maximizing the Bayesian expectation of the complete probability $p(\mathbf{y}, \mathbf{x}, \boldsymbol{\sigma}, \mathbf{u}, \mu^2)$.

1) *E-Step (Inference)*: In this step, the expectation of the complete probability $p(\mathbf{y}, \mathbf{x}, \boldsymbol{\sigma}, \mathbf{u}, \mu^2)$ is computed as

$$\begin{aligned}\mathbb{E}\{p(\mathbf{y}, \mathbf{x}; \boldsymbol{\sigma}, \mathbf{u}, \mu^2)\} &= \mathbb{E}\{\ln p(\mathbf{y}, \mathbf{x}; \boldsymbol{\sigma}, \mathbf{u}, \mu^2)\} \\ &= \mathbb{E}\{\ln p(\mathbf{y}|\mathbf{x}; \mathbf{u}, \mu^2) + \ln p(\mathbf{x}; \boldsymbol{\sigma})\}.\end{aligned}\quad (24)$$

Using (21), (24) can be rewritten as

$$\begin{aligned} & \mathbb{E}\{p(\mathbf{y}, \mathbf{x}; \boldsymbol{\sigma}, \mathbf{u}, \mu^2)\} \\ &= \mathbb{E}\{-N_T \ln \mu^2 - \mu^{-2} \|\mathbf{y} - \mathbf{P}'\mathbf{x}\|_2^2 - \sum_{n=1}^N (\ln \sigma_n + \frac{|x_n|^2}{\sigma_n})\} \\ &= \mathbb{E}\{-N_T \ln \mu^2 - \mu^{-2} \|\mathbf{y} - \mathbf{P}\mathbf{x} - \mathbf{Q}\mathbf{u}\|_2^2 \\ &\quad - \sum_{n=1}^N (\ln \sigma_n + \frac{|x_n|^2}{\sigma_n})\}. \end{aligned} \quad (25)$$

2) *M-Step (Hyperparameter Estimation)*: Now, we consider estimating the hyperparameter set \mathcal{S} by maximizing $\mathbb{E}\{p(\mathbf{y}, \mathbf{x}; \boldsymbol{\sigma}, \mathbf{u}, \mu^2)\}$. To this end, we first compute the partial derivatives of (25) with respect to the unknown parameters as

$$\begin{aligned} & \frac{\partial}{\partial \mathbf{u}} \mathbb{E}\{p(\mathbf{y}, \mathbf{x}; \boldsymbol{\sigma}, \mathbf{u}, \mu^2)\} \\ &= -2\mu^{-2} \left(\mathbb{E}\{\mathbf{Q}^H \mathbf{Q}\} \mathbf{u} - \mathbb{E}\{\mathbf{Q}^H (\mathbf{y} - \mathbf{P}\mathbf{x})\} \right), \end{aligned} \quad (26)$$

$$\frac{\partial}{\partial \mu^2} \mathbb{E}\{p(\mathbf{y}, \mathbf{x}; \boldsymbol{\sigma}, \mathbf{u}, \mu^2)\} = -\frac{N_T}{\mu^2} + \frac{1}{\mu^4} \mathbb{E}\{\|\mathbf{y} - \mathbf{P}'\mathbf{x}\|_2^2\}, \quad (27)$$

$$\frac{\partial}{\partial \sigma_i} \mathbb{E}\{p(\mathbf{y}, \mathbf{x}; \boldsymbol{\sigma}, \mathbf{u}, \mu^2)\} = -\frac{1}{\sigma_n} + \frac{1}{\sigma_n^2} \mathbb{E}\{|x_n|^2\}, \quad (28)$$

where $n \in \mathcal{N} = \{1, \dots, N\}$. By setting the above derivatives to zero, we can get the following expressions

$$\mu^2 = \frac{1}{N_T} \mathbb{E}\{\|\mathbf{y} - \mathbf{P}'\mathbf{x}\|_2^2\}, \quad (29)$$

$$\sigma_n = \mathbb{E}\{|x_n|^2\}, \quad (30)$$

$$\mathbf{u} = \mathbb{E}\{(\mathbf{Q}^H \mathbf{Q})^{-1} \mathbf{Q}^H (\mathbf{y} - \mathbf{P}\mathbf{x})\}, \quad (31)$$

where $\mathbb{E}\{\|\mathbf{y} - \mathbf{P}'\mathbf{x}\|_2^2\}$ in (29) can be written as

$$\mathbb{E}\{\|\mathbf{y} - \mathbf{P}'\mathbf{x}\|_2^2\} = \|\mathbf{y} - \mathbf{P}'\zeta\|_2^2 + \text{Tr}\{\mathbf{P}'\boldsymbol{\Pi}_x\mathbf{P}'^H\}, \quad (32)$$

where $\zeta = \mu^{-2} \boldsymbol{\Pi}_x \mathbf{P}'^H \mathbf{y} \in \mathbb{C}^N$ and $\boldsymbol{\Pi}_x = (\boldsymbol{\Sigma} - \mathbf{S}\mathbf{P}'^H \boldsymbol{\Pi}_y^{-1} \mathbf{P}'\boldsymbol{\Sigma})^{-1} \in \mathbb{C}^{N \times N}$. Furthermore, we have $\mathbf{x}|\mathbf{y} \sim \mathcal{CN}(\zeta, \boldsymbol{\Pi}_x)$, hence (30) becomes $\sigma_n = |\zeta_n|^2$.

By computing (30)-(31) iteratively, one can estimate the parameters $\boldsymbol{\sigma}$, \mathbf{u} and μ^2 . Since the EM algorithm is proved to be convergent [36–39], most of the terms in $\boldsymbol{\sigma}$ and \mathbf{x} converge to 0, yielding to a sparse profile.

Updating \mathbf{u} involves the computation of $(\mathbf{Q}\mathbf{Q})^{-1} \in \mathbb{C}^{N_T^2 \times N_T^2}$ and $\mathbf{Q}(\mathbf{y} - \mathbf{P}\mathbf{x}) \in \mathbb{C}^{N_T^2}$ in (31) which are computationally prohibitive due to large number of unknown parameters, i.e. N_T^2 . Therefore, we propose a low-complexity approach in the sequel.

D. Low-Complexity Approach for Array Perturbation Update

Instead of using an $N_T \times N_T$ full matrix $\mathbf{U}_k[m]$ in (15) to represent the array perturbations, we exploit the LoS-dominant feature of the THz channel, we assume that $L = 1$ by neglecting the NLoS paths, which are approximately 10 dB weaker than the LoS paths [4, 9]. This allows us to model $\mathbf{U}_k[m]$ by a diagonal matrix $\mathbf{C}_k[m]$ instead of a full one. Let us rewrite (16) as

$$\mathbf{a}'_k[m] = \mathbf{C}_k[m] \mathbf{a}_k[m], \quad (33)$$

where $\mathbf{a}'_k[m] \in \mathbb{C}_k^{N_T}$ and $\mathbf{a}_k[m] \in \mathbb{C}^{N_T}$ correspond to the perturbed and nominal array steering vectors, respectively. In (33), $\mathbf{C}_k[m] = \text{diag}(\mathbf{c}_k[m])$ is an $N_T \times N_T$ diagonal transformation matrix. $\mathbf{c}_k[m]$ corresponds to the perturbation due to beam-split and its i th entry can be defined as

$$[\mathbf{c}_k[m]]_i = e^{j\pi(i-1)\Delta_k[m]}, \quad (34)$$

for $i = 2, \dots, N_T$ and $[\mathbf{c}_k]_1[m] = 1$. Notice that this approach involves only a single unknown parameter, i.e., $\Delta_k[m]$ to perform the update from $\mathbf{a}_k[m]$ to $\mathbf{a}'_k[m]$ whereas N_T^2 parameters are involved in (31). Furthermore, the transformation in (33) also allows us to accurately estimate the beam-split as presented in the following lemma.

Lemma 1. *Let $\theta_{k,m}$ be the spatial channel direction, then the beam-split introduced at the m th subcarrier can be uniquely recovered as*

$$\Delta_k[m] = \frac{1}{N_T - 1} \sum_{i=2}^{N_T} \frac{[\mathbf{c}_k]_i[m]}{\pi(i-1)}, \quad (35)$$

where $\angle[\mathbf{c}_k]_i[m]$ is the angle of $[\mathbf{c}_k]_i[m]$.

Proof: Consider the steering vector $\mathbf{a}(\theta_{k,m})$. Then, using (8), the i th entry of $\mathbf{a}(\theta_{k,m})$ is given by

$$[\mathbf{a}(\theta_{k,m})]_i = e^{j\pi(i-1)\theta_{k,m}}. \quad (36)$$

Now, we find the angle of $[\mathbf{a}(\theta_{k,m})]_i$ as $\Omega_{k,i}[m] = \angle[\mathbf{a}(\theta_{k,m})]_i$ for $i = 1, \dots, N_T$. Then, we compute the unwrapped angles as $\boldsymbol{\Omega}_k[m] = \text{unwrap}\{[\Omega_{k,1}[m], \dots, \Omega_{k,N_T}[m]]^T\}$ to ensure not losing information due to the $[-\pi, \pi]$ periodicity of the exponential³. Using $\boldsymbol{\Omega}_k[m]$ and (8), the i th element of the steering vector corresponding to the physical direction $\vartheta_k = \frac{f_c}{f_m} \theta_{k,m}$ becomes

$$[\mathbf{a}(\vartheta_k)]_i = e^{j\Omega_{k,i}[m] \frac{f_c}{f_m}}. \quad (37)$$

Substituting (37) and (36) into (33) yields $[\mathbf{a}(\theta_{k,m})]_i = c_{k,i}[m] [\mathbf{a}(\vartheta_k)]_i$, where the angle of $c_{k,i}[m]$ is given by

$$\begin{aligned} \angle[\mathbf{c}_k[m]]_i &= \Omega_{k,i}[m] \left(1 - \frac{f_c}{f_m}\right) \\ &= \pi(i-1)\theta_{k,m} \left(\frac{\theta_{k,m} - \vartheta_k}{\theta_{k,m}}\right) \\ &= \pi(i-1)\Delta_k[m]. \end{aligned} \quad (38)$$

Then, taking average of $\angle[\mathbf{c}_k[m]]_i$ for $i = 2, \dots, N_T$ and leaving alone $\Delta_k[m]$ leads to (35). ■

Lemma 1 allows us to implement the SBL iterations with significantly lower complexity. The algorithmic steps of our proposed SBCE approach is presented in Algorithm 1. In particular, the SBCE is initialized with ($t = 0$) $\boldsymbol{\sigma}^{(t)} = \mathbf{1}_N$, $\mathbf{C}_k^{(t)}[m] = \mathbf{I}_{N_T}$ and $\mu^{2(t)} = 0$. Then, the covariances $\boldsymbol{\Pi}_y^{(t)}$ and $\boldsymbol{\Pi}_x^{(t)}$ are computed. As the SBCE iterates, $\mathbf{C}_k^{(t)}[m]$ involves the array perturbations due to beam-split and providing a linear transformation between the nominal and actual

³The unwrapped angle information can be easily obtained via the `unwrap` command in MATLAB.

Algorithm 1 SBCE

Input: \mathbf{F} , \mathbf{B} , ϵ_{TH} , f_c , $\mathbf{y}_k[m]$, f_m for $m \in \mathcal{M}$.
Output: $\hat{\mathbf{h}}_k[m]$, $\hat{\vartheta}_k$, $\hat{\Delta}_k[m]$.

- 1: **for** $k \in \mathcal{K}$
- 2: **for** $m \in \mathcal{M}$
- 3: Initialize: $t=0$, $\boldsymbol{\sigma}^{(t)} = \mathbf{1}_N$, $\mathbf{C}_k^{(t)}[m] = \mathbf{I}_{N_T}$ and $\mu^{2(t)} = 0$.
- 4: $\mathbf{y} = \mathbf{y}_k[m]$, $\mathbf{C}^{(t)} = \mathbf{C}_k^{(t)}[m]$, $\mathbf{P}'^{(t)} = \mathbf{B}\mathbf{C}^{(t)}\mathbf{F}$.
- 5: $\text{flag} = \text{true}$.
- 6: **while** $\text{flag} = \text{true}$
- 7: $\boldsymbol{\Sigma}^{(t)} = \text{diag}\{\boldsymbol{\sigma}^{(t)}\}$.
- 8: $\boldsymbol{\Pi}_{\mathbf{y}}^{(t)} = \mathbf{P}'^{(t)}\boldsymbol{\Sigma}^{(t)}\mathbf{P}'^{(t)\text{H}} + \mu^{2(t)}\mathbf{I}_P$.
- 9: $\boldsymbol{\Pi}_{\mathbf{x}}^{(t)} = (\boldsymbol{\Sigma}^{(t)} - \boldsymbol{\Sigma}^{(t)}\mathbf{P}'^{(t)\text{H}}\boldsymbol{\Pi}_{\mathbf{y}}^{(t)\text{-1}}\mathbf{P}'^{(t)}\boldsymbol{\Sigma}^{(t)})^{-1}$.
- 10: $t \leftarrow t + 1$.
- 11: $\boldsymbol{\zeta}^{(t)} = \mu^{2(t)}\boldsymbol{\Pi}_{\mathbf{x}}^{(t)}\mathbf{P}'^{(t)\text{H}}\mathbf{y}$.
- 12: Update $\sigma_n^{(t)} = |\zeta_n^{(t)}|^2$.
- 13: Find $\phi_{n^*}^{(t)}$ from $n^* = \text{argmax}_n |\zeta_n^{(t)}|^2$.
- 14: Construct $\mathbf{a}(\phi_{n^*}^{(t)})$.
- 15: Update $\mathbf{C}^{(t)}$ as $\mathbf{a}(\frac{f_m}{f_c}\phi_{n^*}^{(t)}) = \mathbf{C}^{(t)}\mathbf{a}(\phi_{n^*}^{(t)})$.
- 16: Update $\mathbf{P}'^{(t)} = \mathbf{B}\mathbf{C}^{(t)}\mathbf{F}$.
- 17: Update $\mu^{2(t)} = \frac{1}{N_T} \|\mathbf{y} - \mathbf{P}'^{(t)\text{H}}\boldsymbol{\zeta}^{(t)}\|_2^2 + \text{Tr}\{\mathbf{P}'^{(t)}\boldsymbol{\Pi}_{\mathbf{x}}^{(t)}\mathbf{P}'^{(t)\text{H}}\}$.
- 18: **if** $\|\boldsymbol{\sigma}^{(t)} - \boldsymbol{\sigma}^{(t-1)}\|_2 / \|\boldsymbol{\sigma}^{(t)}\|_2 < \epsilon_{\text{TH}}$
- 19: $\text{flag} = \text{false}$.
- 20: **end if**
- 21: **end while**
- 22: $\mathbf{y}_k[m] = \mathbf{y}$, $\mathbf{C}_k[m] = \mathbf{C}^{(t)}$, $\bar{\vartheta}_k = \phi_{n^*}^{(t)}$.
- 23: Insert $\bar{\vartheta}_k$ into (39)-(43), find the refined directions $\hat{\vartheta}_k$.
- 24: Beam-split estimate: $\hat{\Delta}_k[m] = \frac{1}{N_T-1} \sum_{i=2}^{N_T} \angle\{\frac{[\mathbf{c}_k[m]]_i}{\pi(i-1)}\}$.
- 25: Channel estimate: $\hat{\mathbf{h}}_k[m] = \mathbf{a}(\hat{\vartheta}_k)(\mathbf{B}\mathbf{a}(\hat{\vartheta}_k))^\dagger \mathbf{y}_k[m]$.
- 26: **end for**
- 27: **end for**

steering vectors as $\mathbf{a}(\frac{f_m}{f_c}\phi_{n^*}^{(t)}) = \mathbf{C}^{(t)}\mathbf{a}(\phi_{n^*}^{(t)})$. Once the SBCE converges, the beam-split and the coarse estimate of the physical directions can be obtained. In the following, we discuss refining the estimated physical directions.

E. Refined Direction Estimation

The estimation accuracy of the direction estimates obtained via the support of \mathbf{x} is subject to the angular resolution of the selected grid, i.e., $\rho = \frac{1}{N}$. Hence, once the EM algorithm terminates, we use the resulting estimates and search for the refined directions by employing a finer grid [36, 37]. Let us define the finer grid for the l th physical direction ϑ_l as $\Phi_l = [\vartheta_l - \varphi, \vartheta_l + \varphi]$, where the grid interval is 2φ . Then, we rewrite the covariance of the received signal $\boldsymbol{\Pi}_{\mathbf{y}}$ as

$$\boldsymbol{\Pi}_{\mathbf{y}} = \boldsymbol{\Pi}_{\mathbf{y}\setminus l} + \eta_l \mathbf{g}'(\vartheta_l) \mathbf{g}'^{\text{H}}(\vartheta_l), \quad (39)$$

where $\mathbf{g}'(\vartheta_l) = \mathbf{B}\mathbf{C}\mathbf{a}(\vartheta_l) \in \mathbb{C}^P$ and η_l is the power of the l th signal. $\boldsymbol{\Pi}_{\mathbf{y}\setminus l}$ denotes to the covariance matrix in (23) by excluding the columns of \mathbf{P}' corresponding to ϑ_l . By

substituting (39) into (22), we can obtain the refined directions via $\{\hat{\vartheta}_l, \hat{\eta}_l\} = \arg \max_{\eta_l, \vartheta_l} f(\eta_l, \vartheta_l)$, where $f(\eta_l, \vartheta_l)$ is

$$f(\eta_l, \vartheta_l) = \frac{1}{|\pi[\boldsymbol{\Pi}_{\mathbf{y}\setminus l} + \eta_l \mathbf{g}'(\vartheta_l) \mathbf{g}'^{\text{H}}(\vartheta_l)]|} \times \exp \left\{ -\text{Tr} \left\{ [\boldsymbol{\Pi}_{\mathbf{y}\setminus l} + \eta_l \mathbf{g}'(\vartheta_l) \mathbf{g}'^{\text{H}}(\vartheta_l)]^{-1} \mathbf{R}_{\mathbf{y}} \right\} \right\}. \quad (40)$$

To simplify (40), we first set the derivative $\frac{\partial f(\eta_l, \vartheta_l)}{\partial \eta_l}$ to zero, which yields

$$\hat{\eta}_l = \frac{\mathbf{g}'^{\text{H}}(\vartheta_l) \boldsymbol{\Pi}_{\mathbf{y}\setminus l}^{-1} (\mathbf{R}_{\mathbf{y}} - \boldsymbol{\Pi}_{\mathbf{y}\setminus l}) \boldsymbol{\Pi}_{\mathbf{y}\setminus l}^{-1} \mathbf{g}'(\vartheta_l)}{[\mathbf{g}'^{\text{H}}(\vartheta_l) \boldsymbol{\Pi}_{\mathbf{y}\setminus l}^{-1} \mathbf{g}'(\vartheta_l)]}, \quad (41)$$

and insert (41) into $\frac{\partial f(\eta_l, \vartheta_l)}{\partial \vartheta_l} = 0$. Then, we get

$$\begin{aligned} \text{Re}\{\mathbf{g}'^{\text{H}}(\vartheta_l) \boldsymbol{\Pi}_{\mathbf{y}\setminus l}^{-1} [\mathbf{g}'(\vartheta_l) \mathbf{g}'^{\text{H}}(\vartheta_l) \boldsymbol{\Pi}_{\mathbf{y}\setminus l}^{-1} \mathbf{R}_{\mathbf{y}} \\ - \mathbf{R}_{\mathbf{y}} \boldsymbol{\Pi}_{\mathbf{y}\setminus l}^{-1} \mathbf{g}'(\vartheta_l) \mathbf{g}'^{\text{H}}(\vartheta_l)] \boldsymbol{\Pi}_{\mathbf{y}\setminus l}^{-1} \mathbf{g}'(\vartheta_l)\} = 0, \end{aligned} \quad (42)$$

where $\dot{\mathbf{g}}'(\vartheta_l) = \frac{\partial \mathbf{g}'(\vartheta_l)}{\partial \vartheta_l}$. Using (42), we can write the refined direction estimation problem as

$$\begin{aligned} \hat{\vartheta}_l = \arg \max_{\vartheta_l} |\text{Re}\{\mathbf{g}'^{\text{H}}(\vartheta_l) \boldsymbol{\Pi}_{\mathbf{y}\setminus l}^{-1} [\mathbf{g}'(\vartheta_l) \mathbf{g}'^{\text{H}}(\vartheta_l) \boldsymbol{\Pi}_{\mathbf{y}\setminus l}^{-1} \mathbf{R}_{\mathbf{y}} \\ - \mathbf{R}_{\mathbf{y}} \boldsymbol{\Pi}_{\mathbf{y}\setminus l}^{-1} \mathbf{g}'(\vartheta_l) \mathbf{g}'^{\text{H}}(\vartheta_l)] \boldsymbol{\Pi}_{\mathbf{y}\setminus l}^{-1} \mathbf{g}'(\vartheta_l)\}|^{-1}. \end{aligned} \quad (43)$$

F. Computational Complexity

The computational complexity of our proposed SBCE is mainly due to the matrix computations in Algorithm 1, which are $O(PN^2 + NP^2)$ (Step 8), $O(2N^2P + NP^2 + 2N^3 + P^3)$ (Step 9), $O(N^2P + NP)$ (Step 11), $O(P^2N_T^3N)$ (Step 16) and $O(NP + PN^2 + P^2N)$ (Step 17), respectively. Hence, the overall complexity order of the proposed SBCE approach is $O(T[PN(5N^2 + 3P^2 + PN_T^3 + 2) + 2P^3 + 3N^3])$, where T is the total number of iterations.

IV. NEAR-FIELD CONSIDERATIONS

Due to operating at high frequencies as well as employing extremely small array aperture, THz-band transmission may encounter near-field phenomenon for close-proximity users. Specifically, in the far-field the transmitted signal reaches to the users as plane-wave whereas the plane wavefront is spherical in the near-field when the transmission range is shorter than the Rayleigh distance, i.e., $R = \frac{2G^2f_c}{c_0}$ where G is the array aperture [2, 50]. For ULA, we have $G = (N_T - 1)\frac{c_0}{2f_c}$, for which the Rayleigh distance becomes $R \approx \frac{N_T^2 c_0}{2f_c}$ for large N_T .

Compared to its far-field counterpart, the near-field model involves additional range parameter. In particular, the i th element of the steering vectors for ULA in near- and far-field can be given by [34, 50]

$$[\mathbf{a}_{\text{NF}}(\vartheta, r)]_i = e^{-j2\pi \frac{f_m}{c_0} [r^{(i)} - r]} \quad (44)$$

$$[\mathbf{a}_{\text{FF}}(\vartheta)]_i = e^{j2\pi \frac{f_m}{c_0} \vartheta}, \quad (45)$$

where r ($r^{(i)}$) stands for the distance between the user and array origin (the i th BS antenna). In (44), $r^{(i)}$ is defined by

$$\begin{aligned} r^{(i)} &= [r^2 + ((i-1)\bar{d})^2 - 2(i-1)\bar{d}r\vartheta]^{\frac{1}{2}}, \\ &\approx r - (i-1)\bar{d}\vartheta, \end{aligned} \quad (46)$$

where the approximation can be achieved by utilizing the Taylor expansion [4, 30, 34].

Now, we calculate beam-split in near-field. Using the approximated model in (46), and $\bar{d} = \frac{c_0}{2f_c}$, we rewrite (44) as

$$\begin{aligned} [\mathbf{a}_{\text{NF}}(\vartheta, r)]_i &= e^{-j2\pi\frac{f_m}{c_0}(r(i-1)\bar{d}\vartheta)} \\ &= e^{-j\pi(i-1)\frac{f_m}{f_c}r\vartheta} \\ &= e^{-j\pi(i-1)\theta}, \end{aligned} \quad (47)$$

where $\theta_{r,m} = \frac{f_m}{f_c}r\vartheta$ denotes the near-field spatial channel direction and the near-field beam split can be defined as

$$\Delta_{r,m} = \theta_{r,m} - \vartheta = \left(\frac{f_m}{f_c}r - 1\right)\vartheta. \quad (48)$$

V. SBFL FOR THZ CHANNEL ESTIMATION

Using the channel estimate via SBCE, we develop an FL scheme for THz channel estimation in this part. In FL, the users collaborate on training a learning model by computing the model parameters based on their local datasets [51]. Let $\xi \in \mathbb{R}^Q$ and \mathcal{D}_k be the set of model parameters and the local dataset of the k th user, respectively. Then, the trained model provides a nonlinear relationship, $f(\xi)$ between the input and output as $\mathcal{Y}_k^{(i)} = f(\xi)\mathcal{X}_k^{(i)}$ for $i = 1, \dots, \mathcal{D}_k$, where $\mathcal{D}_k = |\mathcal{D}_k|$ is the number of samples in the k th local dataset. Here, $\mathcal{X}_k^{(i)}$ and $\mathcal{Y}_k^{(i)}$ are the input and output data for the i th sample of the k th dataset with $\mathcal{D}_k^{(i)} = (\mathcal{X}_k^{(i)}, \mathcal{Y}_k^{(i)})$.

A. Data Collection and Training

During the dataset collection, each user collects its own training dataset from the received pilots. Given the channel estimate $\hat{\mathbf{h}}_k[m]$, the output data is given by $\mathcal{Y}_k = \left[\text{Re}\{\hat{\mathbf{h}}_k[m]\}^\top, \text{Im}\{\hat{\mathbf{h}}_k[m]\}^\top\right]^\top \in \mathbb{R}^{2N_T}$. The input data $\mathcal{X}_k \in \mathbb{R}^{P \times 3}$ includes the real, imaginary and angle information of $\mathbf{y}_k[m]$ to yield improved feature representation [51]. Thus, we have $[\mathcal{X}_k]_1 = \text{Re}\{\mathbf{y}_k[m]\}$, $[\mathcal{X}_k]_2 = \text{Im}\{\mathbf{y}_k[m]\}$ and $[\mathcal{X}_k]_3 = \angle\{\mathbf{y}_k[m]\}$.

Then, the FL problem becomes

$$\begin{aligned} \min_{\xi} \quad & \frac{1}{K} \sum_{k=1}^K \mathcal{L}_k(\xi) \\ \text{subject to:} \quad & f(\mathcal{X}_k^{(i)}|\xi) = \mathcal{Y}_k^{(i)}, \end{aligned} \quad (49)$$

for $i = 1, \dots, \mathcal{D}_k$ and $k = 1, \dots, K$. In (49), $\mathcal{L}_k(\xi) = \frac{1}{\mathcal{D}_k} \sum_{i=1}^{\mathcal{D}_k} \|f(\mathcal{X}_k^{(i)}|\xi) - \mathcal{Y}_k^{(i)}\|_F^2$ corresponds to the loss function at the k th user and $f(\mathcal{X}_k^{(i)}|\xi)$ denotes model prediction given the input $\mathcal{X}_k^{(i)}$. To efficiently solve (49), gradient descent is employed and the problem is solved iteratively, wherein the model parameter update is performed at the j th iteration as $\xi_{t+1} = \xi_j - \eta \frac{1}{K} \sum_{k=1}^K \beta_k(\xi_j)$ for $j = 1, \dots, J$. Here, $\beta_k(\xi_j) = \nabla \mathcal{L}_k(\xi_j) \in \mathbb{R}^Q$ is the gradient vector and η is the learning rate.

B. Communication Overhead

The communications overhead of both FL and CL can be given as the amount of data transmitted during training [52, 53], i.e., $\mathcal{T}_{\text{FL}} = 2QJK$ and $\mathcal{T}_{\text{CL}} = \sum_{k=1}^K \mathcal{D}_k(3P + 2N_T)$, respectively. Here, \mathcal{T}_{FL} involves transmission of model parameters of K users for T iterations, while \mathcal{T}_{CL} is computed as the size of dataset of K users.

VI. NUMERICAL EXPERIMENTS

In this section, the performance of our proposed SBCE approach is evaluated in comparison with the state-of-the-art techniques, e.g., LS and MMSE in (11), GSOMP [30], OMP, BSPD [19] and BSA [31], in terms of NMSE, calculated as $\text{NMSE} = \frac{1}{J_T K M} \sum_{i=1, k=1, m=1}^{J_T, K, M} \frac{\|\mathbf{h}_k[m] - \hat{\mathbf{h}}_k^{(i)}[m]\|_2^2}{\|\mathbf{h}_k[m]\|_2^2}$, where $J_T = 100$ is the number of Monte Carlo trials. During simulations, the THz channel scenario is realized based on the channel model in (4) with $f_c = 300$ GHz, $B = 30$ GHz, $M = 128$, $N_T = 256$, $N_{\text{RF}} = P = 32$, $L = 1$, $K = 8$ and $\tilde{\vartheta}_k \in [-\frac{\pi}{2}, \frac{\pi}{2}]$ [4, 5, 19]. The overcomplete dictionary matrix \mathbf{F} is constructed for $N = 3N_T$, and $[\mathbf{B}]_{i,j} = \frac{1}{\sqrt{N_T}} e^{j\tilde{\vartheta}_k}$, where $\tilde{\vartheta}_k \sim \text{uniform}(-1, 1)$. The proposed SBCE algorithm is initialized with $\sigma^{(0)} = \mathbf{1}_N$, $\mathbf{C}_k^{(0)}[m] = \mathbf{I}_{N_T}$, $\mu^{2(0)} = 0$, and run as presented in Algorithm 1. The termination parameter is selected as $\epsilon_{\text{TH}} = 0.001$. It is observed that the SBCE algorithm converges in approximately $T = 50$ iterations.

For SBFL, data generation and training are handled over an hyperparameter optimization of the learning model in the FL toolbox in MATLAB on a PC with a 2304-core GPU. We design a CNN with 12 layers and $Q = 603,648$ parameters [52]. The first layer accepts the input of size $P \times 3$. The $\{2, 4, 6, 8\}$ th layers are convolutional layers with 128 filters of size 3×3 . The $\{3, 5, 7, 9\}$ th layers are normalization layers. The 10th layer is a fully connected layer with 1024 units, following with a dropout layer with 50% probability. Finally, the 12th layer is the output layer of size $2N_T \times 1$. The CNN model is trained for $J = 100$ iterations with the learning rate $\eta = 0.001$. During data generation, we generated 100 channel realizations, and we added AWGN on the input data for three signal-to-noise ratio (SNR) levels, i.e., $\text{SNR} = \{15, 20, 25\}$ dB for 50 realizations to provide robust performance [52].

Fig. 2 shows the NMSE performance of the competing algorithms with respect to SNR. We observe that the proposed SBCE approach attains better NMSE as compared to other algorithmic-based approaches, i.e., BSA and BSPD. The direct application of both OMP and LS yields poor NMSE since they do not involve any specific mechanism to mitigate beam-split. While BSPD and BSA are beam-split-aware techniques, they suffer from inaccurate support detection, which leads to precision loss as SNR increases. The proposed SBCE approach has very close performance to GSOMP which employs additional TD hardware. In addition, we present the physical channel direction estimation RMSE in Fig. 3. While both the proposed SBCE approach and GSOMP follows the CRB closely, the remaining methods suffer from grid error and yield approximately 0.1° RMSE. Comparing SBCE and SBFL, we observe that the latter has slight performance loss as well as it suffers from low NMSE in high SNR. This is because of the

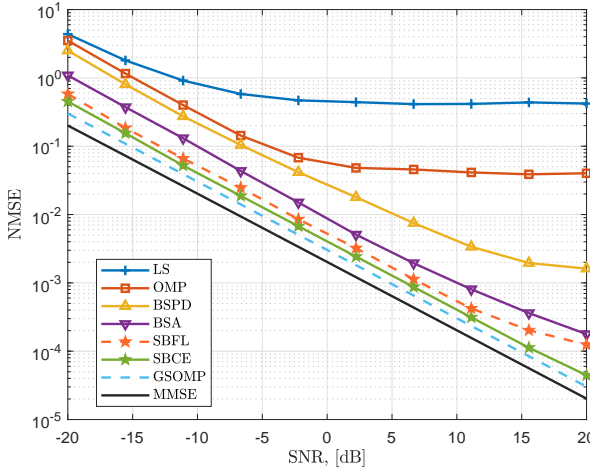


Fig. 2. Channel estimation NMSE versus SNR.

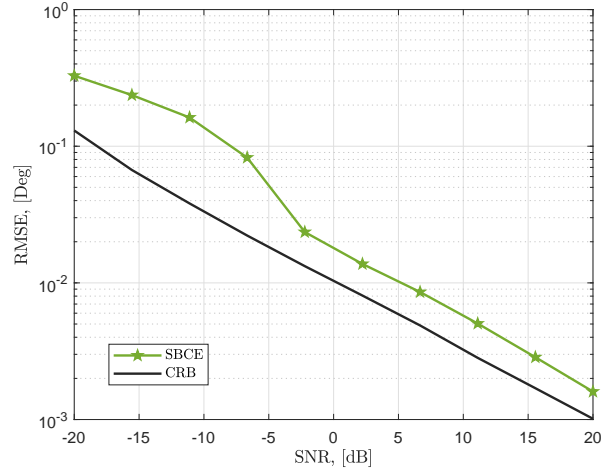


Fig. 4. Beam-split estimation RMSE versus SNR.

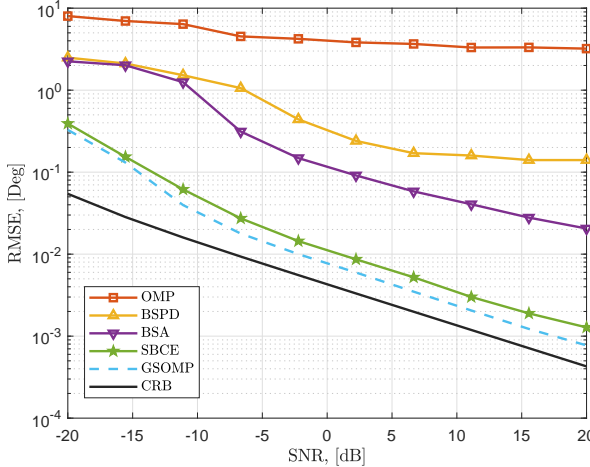


Fig. 3. Physical channel direction RMSE versus SNR.

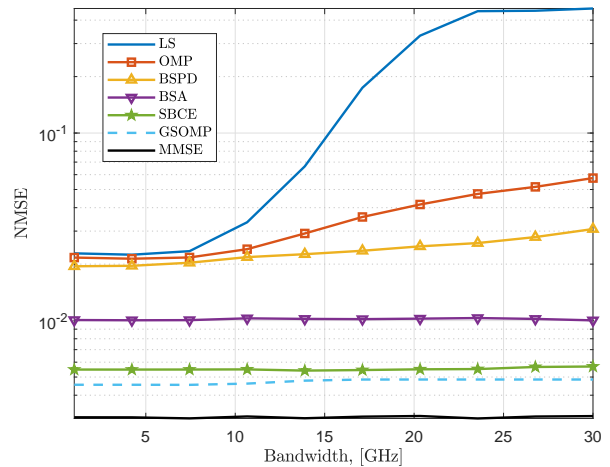


Fig. 5. Channel estimation NMSE against bandwidth.

neural network losing precision due to decentralize learning and noisy dataset to prove robustness against imperfect data.

In Fig. 4, beam-split estimation RMSE is shown with respect to SNR. As it is seen, the proposed approach effectively estimates the beam-split and follows the statistical lower bound CRB with a slight performance gap (e.g., $\sim 0.01^\circ$ in 0 dB). The channel estimation techniques, i.e., GSOMP, BSPD and BSA, however, do not have the capability to obtain the beam-split.

Fig. 5 shows the channel estimation NMSE against bandwidth for the interval of [1, 30] GHz at 300 GHz carrier frequency. We can see that all of the algorithms provide approximately 0.02 NMSE for the bandwidth $B < 7$ GHz. However, the performance of LS and OMP degrades as the bandwidth widens since these method do not involve beam-split mitigation. Also, BSPD yields a slight NMSE loss at wide bandwidth while BSA has robust performance. On the other hand, the proposed SBCE method enjoys robustness against

the increase of the bandwidth and provides close to NMSE performance along with GSOMP.

Finally, we investigate the deviation from far-field model in terms of transmission range and frequency. Fig. 6a shows the difference between near- and far-field steering vectors with respect to transmission range for various frequencies and corresponding Rayleigh distances. As it is seen, the NMSE curve crosses the Rayleigh distance approximately at 0.0013 for all frequencies at different ranges. Specifically, NMSE crosses the Rayleigh distance at 32 m for $f_c = 300$ GHz, which shows that the near-field model should be considered for $r < 32$ m when $N_T = 256$. Note that this distance is smaller if rectangular arrays are used. For instance, a 16×16 URA has the array aperture of $G = 16\sqrt{2d}$ leading to $R = 0.256$ m, which yields much safer use of far-field model in shorter distance. Fig. 6b illustrates the channel estimation NMSE with respect to transmission range when far-field model is used in GSOMP and SBCE. We observe that relatively large error

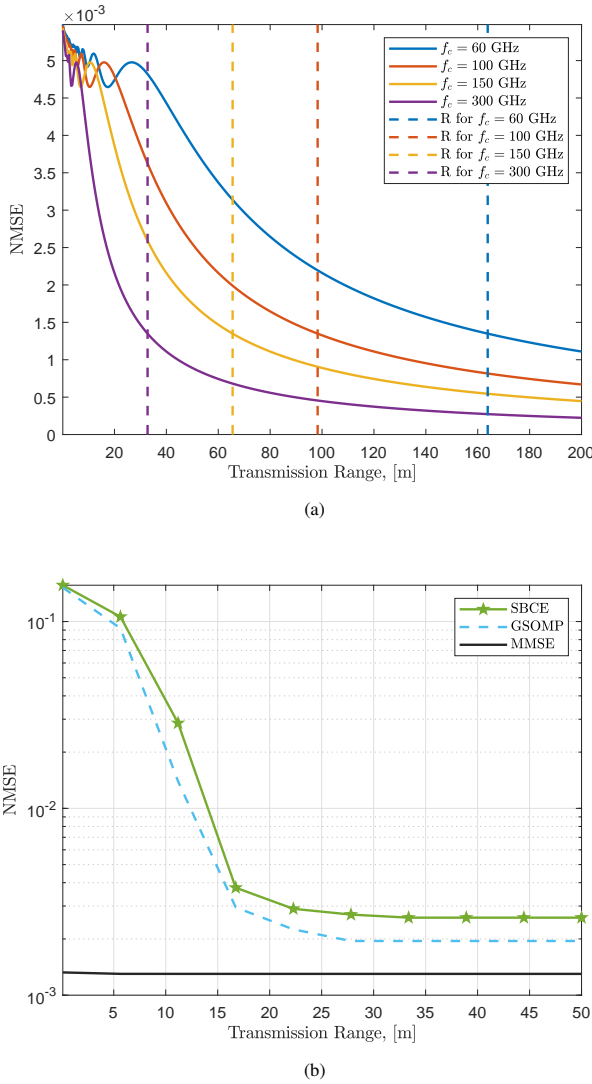


Fig. 6. (a) NMSE between near- and far-field steering vectors, and (b) channel estimation NMSE for the usage of far-field model with respect to transmission range.

for $r < R$ due to mismatch between the far- and near-field steering vectors. Although fixing the direction information may yield less error [30], which only due to range-mismatch, the mismatch in the range also causes inaccurate direction estimates.

VII. CONCLUSIONS

In this work, we proposed an SBL-based approach for joint THz channel and beam-split estimation. The proposed method is based on modeling the beam-split as an array perturbation. We have shown that the proposed SBCE approach effectively estimates THz channel as compared to existing methods without requiring additional hardware components such as TD networks. The SBCE technique is also capable of effectively estimating the beam-split. This is particularly helpful to design the hybrid beamformers more easily with the knowledge of beam-split. Also, a model-free technique, SBFL, is introduced to realize the problem from ML perspective for computational- and communication-efficiency. Furthermore, we examined the

near-field considerations of the THz channel and evaluate the performance of SBCE with far-field model. The estimation of the near-field THz channel is one particular problem that we reserve to study for future work.

APPENDIX A CRAMÉR-RAO LOWER BOUND

In order to derive the CRB, we assume a single user case, i.e., $K = 1$ without loss of generality. The CRB expressions can easily be extended for the $K > 1$ case by using the decoupledness of the unknown parameters of multiple users. Now, let us define the unknown parameter vector as the physical directions and beam-splits corresponding to L paths. Hence, we have a $2L \times 1$ unknown vector as

$$\mathbf{v} = [\vartheta_1, \dots, \vartheta_L, \Delta_1, \dots, \Delta_L]^T \in \mathbb{C}^{2L}. \quad (50)$$

Consider the log-likelihood function of the joint pdf in (22) with respect to \mathbf{v} as

$$\mathcal{L}(\mathbf{v}) = \ln\{p(\mathbf{y}|\mathbf{v})\} = -\ln|\mathbf{\Pi}_y| - \text{Tr}\{\mathbf{\Pi}_y^{-1}\mathbf{R}_y\}. \quad (51)$$

In order to obtain the CRB, we first need to find the Fisher information matrix (FIM), which measures the amount of information contained for the unknown variables. Let $\mathbf{FIM} \in \mathbb{R}^{2L \times 2L}$ be the FIM. Then, the (i, j) th entry of \mathbf{FIM} is calculated as the second derivative of $\mathcal{L}(\mathbf{v})$ as

$$[\mathbf{FIM}]_{ij} = -\mathbb{E}\left\{\frac{\partial^2 \mathcal{L}(\mathbf{v})}{\partial v_i \partial v_j}\right\}, \quad (52)$$

for $i, j = 1, \dots, 2L$. Let us calculate the first derivatives of $\mathcal{L}(\mathbf{v})$. Using

$$\begin{aligned} \frac{\partial \ln\{|\mathbf{\Pi}_y|\}}{\partial v_i} &= \text{Tr}\left\{\mathbf{\Pi}_y^{-1} \frac{\partial \mathbf{\Pi}_y}{\partial v_i}\right\} \\ \frac{\partial \mathbf{\Pi}_y^{-1}}{\partial v_i} &= -\mathbf{\Pi}_y^{-1} \frac{\partial \mathbf{\Pi}_y}{\partial v_i} \mathbf{\Pi}_y^{-1}, \end{aligned} \quad (53)$$

we get the first derivative of $\mathcal{L}(\mathbf{v})$ as

$$\begin{aligned} \frac{\partial \mathcal{L}(\mathbf{v})}{\partial v_i} &= -\text{Tr}\left\{\mathbf{\Pi}_y^{-1} \frac{\partial \mathbf{\Pi}_y}{\partial v_i}\right\} + \mathbf{\Pi}_y^{-1} \frac{\partial \mathbf{\Pi}_y}{\partial v_i} \mathbf{\Pi}_y^{-1} \mathbf{R}_y \\ &= \text{Tr}\left\{\left(\mathbf{\Pi}_y^{-1} \frac{\partial \mathbf{\Pi}_y}{\partial v_i}\right) (\mathbf{\Pi}_y^{-1} \mathbf{R}_y - \mathbf{I}_P)\right\}, \end{aligned} \quad (54)$$

and the second derivative becomes

$$\begin{aligned} \frac{\partial^2 \mathcal{L}(\mathbf{v})}{\partial v_i \partial v_j} &= \text{Tr}\left\{\frac{\partial}{\partial v_j} \left(\mathbf{\Pi}_y^{-1} \frac{\partial \mathbf{\Pi}_y}{\partial v_i}\right) (\mathbf{\Pi}_y^{-1} \mathbf{R}_y - \mathbf{I}_P)\right\} \\ &\quad + \left(\mathbf{\Pi}_y^{-1} \frac{\partial \mathbf{\Pi}_y}{\partial v_i}\right) \frac{\partial}{\partial v_j} (\mathbf{\Pi}_y^{-1} \mathbf{R}_y - \mathbf{I}_P) \\ &= \text{Tr}\left\{\frac{\partial}{\partial v_j} \left(\mathbf{\Pi}_y^{-1} \frac{\partial \mathbf{\Pi}_y}{\partial v_i}\right) (\mathbf{\Pi}_y^{-1} \mathbf{R}_y - \mathbf{I}_P)\right\} \\ &\quad + \left(\mathbf{\Pi}_y^{-1} \frac{\partial \mathbf{\Pi}_y}{\partial v_i}\right) \frac{\partial}{\partial v_j} \mathbf{\Pi}_y^{-1} \frac{\partial \mathbf{\Pi}_y}{\partial v_j} \mathbf{\Pi}_y^{-1} \mathbf{R}_y. \end{aligned} \quad (55)$$

Since $\mathbb{E}\{\mathbf{R}_y\} = \mathbf{\Pi}_y$, (52) can be rewritten as

$$[\mathbf{FIM}]_{ij} = -\mathbb{E}\left\{\frac{\partial^2 \mathcal{L}(\mathbf{v})}{\partial v_i \partial v_j}\right\} = \text{Tr}\left\{\frac{\partial}{\partial v_i} \mathbf{\Pi}_y^{-1} \frac{\partial \mathbf{\Pi}_y}{\partial v_j} \mathbf{\Pi}_y^{-1} \mathbf{R}_y\right\}, \quad (56)$$

which is the general FIM expression for Gaussian signals. Then, by following the steps in [35, 54], the CRB expressions corresponding to the (i, j) th entries of the FIM can be given by

$$\text{CRB}_{ij} = \frac{1}{\frac{2}{\mu^2} \text{Tr}\{\mathbf{M}\mathbf{K}_{ij}\}}, \quad (57)$$

where $\mathbf{M} = \bar{\Sigma}^H \mathbf{A}'^H \Pi_y^{-1} \mathbf{A}' \bar{\Sigma} \in \mathbb{C}^{L \times L}$, where $\bar{\Sigma}$ is an $L \times L$ matrix comprised of signal powers. $\mathbf{K}_{ij} \in \mathbb{C}^{L \times L}$ includes the derivative of the actual steering matrix \mathbf{A}' with respect to the unknown parameters, and it is given by

$$\mathbf{K}_{ij} = \left[\frac{\partial \mathbf{A}'}{\partial v_i} \right]^H (\mathbf{I}_{N_T} - \mathbf{A}' \mathbf{A}'^{\dagger}) \left[\frac{\partial \mathbf{A}'}{\partial v_j} \right]. \quad (58)$$

In particular, the i th entry of the derivative of $\mathbf{a}'(\vartheta_l)$, i.e., the l th column of \mathbf{A}' with respect to the physical direction ϑ_l and beam-split Δ_l are respectively given by

$$\frac{\partial [\mathbf{a}']_i}{\partial \vartheta_l} = j\pi(i-1) \frac{f_m}{f_c} \cos \tilde{\vartheta}_l [\mathbf{a}']_i, \quad (59)$$

$$\frac{\partial [\mathbf{a}']_i}{\partial \Delta_l} = j\pi(i-1) e^{j\pi(i-1) \sin \tilde{\vartheta}_l} [\mathbf{a}']_i, \quad (60)$$

where we have via (6) and (8) that $[\mathbf{a}']_i = e^{j\pi(i-1) \frac{f_m}{f_c} \sin \tilde{\vartheta}_l} = e^{j\pi(i-1)(\Delta_l + \sin \tilde{\vartheta}_l)}$.

In case of near-field scenario, the derivatives of the steering vector in (47) with respect to ϑ_l , r_l and near-field beam-split $\Delta_{l,r}$ are

$$\frac{\partial [\mathbf{a}'_{\text{NF}}]_i}{\partial \vartheta_l} = -j\pi(i-1) \frac{f_m}{f_c} r \cos \tilde{\vartheta}_l [\mathbf{a}'_{\text{NF}}]_i, \quad (61)$$

$$\frac{\partial [\mathbf{a}'_{\text{NF}}]_i}{\partial r_l} = -j\pi(i-1) \frac{f_m}{f_c} \sin \tilde{\vartheta}_l [\mathbf{a}'_{\text{NF}}]_i, \quad (62)$$

$$\frac{\partial [\mathbf{a}'_{\text{NF}}]_i}{\partial \Delta_{l,r}} = -j\pi r(i-1) e^{j\pi r(i-1) \sin \tilde{\vartheta}_l} [\mathbf{a}'_{\text{NF}}]_i. \quad (63)$$

REFERENCES

- [1] K. B. Letaief, Y. Shi, J. Lu, and J. Lu, "Edge artificial intelligence for 6G: Vision, enabling technologies, and applications," *IEEE J. Sel. Areas Commun.*, vol. 40, no. 1, pp. 5–36, 2021.
- [2] I. F. Akyildiz, C. Han, Z. Hu, S. Nie, and J. M. Jornet, "Terahertz Band Communication: An Old Problem Revisited and Research Directions for the Next Decade," *IEEE Trans. Commun.*, vol. 70, no. 6, pp. 4250–4285, May 2022.
- [3] Z. Chen, C. Han, Y. Wu, L. Li, C. Huang, Z. Zhang, G. Wang, and W. Tong, "Terahertz Wireless Communications for 2030 and Beyond: A Cutting-Edge Frontier," *IEEE Commun. Mag.*, vol. 59, no. 11, pp. 66–72, Nov. 2021.
- [4] H. Sarieddeen, M.-S. Alouini, and T. Y. Al-Naffouri, "An overview of signal processing techniques for Terahertz communications," *Proceedings of the IEEE*, vol. 109, no. 10, pp. 1628–1665, 2021.
- [5] A. M. Elbir, K. V. Mishra, and S. Chatzinotas, "Terahertz-Band Joint Ultra-Massive MIMO Radar-Communications: Model-Based and Model-Free Hybrid Beamforming," *IEEE J. Sel. Top. Signal Process.*, vol. 15, no. 6, pp. 1468–1483, Oct. 2021.
- [6] A. M. Elbir, K. V. Mishra, S. Chatzinotas, and M. Bennis, "Terahertz-Band Integrated Sensing and Communications: Challenges and Opportunities," *arXiv*, Aug. 2022.
- [7] H. Yuan, N. Yang, K. Yang, C. Han, and J. An, "Hybrid Beamforming for Terahertz Multi-Carrier Systems Over Frequency Selective Fading," *IEEE Trans. Commun.*, vol. 68, no. 10, pp. 6186–6199, Jul 2020.
- [8] J. Tan and L. Dai, "Wideband Beam Tracking in THz Massive MIMO Systems," *IEEE J. Sel. Areas Commun.*, vol. 39, no. 6, pp. 1693–1710, Apr. 2021.
- [9] S. Tarboush, H. Sarieddeen, H. Chen, M. H. Loukil, H. Jemaa, M. S. Alouini, and T. Y. Al-Naffouri, "TeraMIMO: A Channel Simulator for Wideband Ultra-Massive MIMO Terahertz Communications," *arXiv*, Apr 2021.
- [10] H. Sarieddeen, M.-S. Alouini, and T. Y. Al-Naffouri, "Terahertz-band ultra-massive spatial modulation MIMO," *IEEE J. Sel. Areas Commun.*, vol. 37, no. 9, pp. 2040–2052, 2019.
- [11] A. Faisal, H. Sarieddeen, H. Dahrouj, T. Y. Al-Naffouri, and M.-S. Alouini, "Ultramassive MIMO systems at Terahertz bands: Prospects and challenges," *IEEE Veh. Technol. Mag.*, vol. 15, no. 4, pp. 33–42, 2020.
- [12] B. Ning, Z. Chen, W. Chen, Y. Du, and J. Fang, "Terahertz Multi-User Massive MIMO With Intelligent Reflecting Surface: Beam Training and Hybrid Beamforming," *IEEE Trans. Veh. Technol.*, vol. 70, no. 2, pp. 1376–1393, Jan 2021.
- [13] B. Wang, M. Jian, F. Gao, G. Y. Li, and H. Lin, "Beam Squint and Channel Estimation for Wideband mmWave Massive MIMO-OFDM Systems," *IEEE Trans. Signal Process.*, vol. 67, no. 23, pp. 5893–5908, Oct. 2019.
- [14] C. Lin and G. Y. Li, "Terahertz Communications: An Array-of-Subarrays Solution," *IEEE Commun. Mag.*, vol. 54, no. 12, pp. 124–131, Dec 2016.
- [15] O. E. Ayach, S. Rajagopal, S. Abu-Surra, Z. Pi, and R. W. Heath, "Spatially sparse precoding in millimeter wave MIMO systems," *IEEE Trans. Wireless Commun.*, vol. 13, no. 3, pp. 1499–1513, 2014.
- [16] R. W. Heath, N. González-Prelcic, S. Rangan, W. Roh, and A. M. Sayeed, "An overview of signal processing techniques for millimeter wave MIMO systems," *IEEE J. Sel. Topics Signal Process.*, vol. 10, no. 3, pp. 436–453, 2016.
- [17] R. Méndez-Rial, C. Rusu, A. Alkhateeb, N. González-Prelcic, and R. W. Heath, "Channel estimation and hybrid combining for mmWave: Phase shifters or switches?" in *IEEE Information Theory and Applications Workshop*, 2015, pp. 90–97.
- [18] A. Alkhateeb, G. Leus, and R. W. Heath, "Limited feedback hybrid precoding for multi-user millimeter wave systems," *IEEE Trans. Wireless Commun.*, vol. 14, no. 11, pp. 6481–6494, 2015.
- [19] J. Tan and L. Dai, "Wideband channel estimation for THz massive MIMO," *China Commun.*, vol. 18, no. 5, pp. 66–80, May 2021.
- [20] J. Tan and L. Dai, "THz Precoding for 6G: Challenges, Solutions, and Opportunities," *IEEE Wireless Commun.*, pp. 1–8, May 2022.
- [21] B. Wang, F. Gao, S. Jin, H. Lin, G. Y. Li, S. Sun, and T. S. Rappaport, "Spatial-Wideband Effect in Massive MIMO with Application in mmWave Systems," *IEEE Commun. Mag.*, vol. 56, no. 12, pp. 134–141, Aug 2018.
- [22] M. Wang, F. Gao, N. Shlezinger, M. F. Flanagan, and Y. C. Eldar, "A Block Sparsity Based Estimator for mmWave Massive MIMO Channels With Beam Squint," *IEEE Trans. Signal Process.*, vol. 68, pp. 49–64, Nov 2019.
- [23] A. Brighente, M. Cerutti, M. Nicoli, S. Tomasin, and U. Spagnolini, "Estimation of Wideband Dynamic mmWave and THz Channels for 5G Systems and Beyond," *IEEE J. Sel. Areas Commun.*, vol. 38, no. 9, pp. 2026–2040, Jun 2020.
- [24] S. Srivastava, A. Tripathi, N. Varshney, A. K. Jagannatham, and L. Hanzo, "Hybrid Transceiver Design for Tera-Hertz MIMO Systems Relying on Bayesian Learning Aided Sparse Channel Estimation," *arXiv*, Sep. 2021.
- [25] W. Yu, Y. Shen, H. He, X. Yu, J. Zhang, and K. B. Letaief, "Hybrid Far- and Near-Field Channel Estimation for THz Ultra-Massive MIMO via Fixed Point Networks," *arXiv*, May 2022.
- [26] E. Balevi and J. G. Andrews, "Wideband Channel Estimation With a Generative Adversarial Network," *IEEE Trans. Wireless Commun.*, vol. 20, no. 5, pp. 3049–3060, Jan. 2021.
- [27] B. Peng, S. Wessemann, K. Guan, W. Templ, and T. Kürner, "Precoding and Detection for Broadband Single Carrier Terahertz Massive MIMO Systems Using LSQR Algorithm," *IEEE Trans. Wireless Commun.*, vol. 18, no. 2, pp. 1026–1040, Jan. 2019.
- [28] S. Nie and I. F. Akyildiz, "Deep Kernel Learning-Based Channel Estimation in Ultra-Massive MIMO Communications at 0.06–10 THz," in *2019 IEEE Globecom Workshops (GC Wkshps)*. IEEE, Dec. 2019, pp. 1–6.
- [29] Y. Chen and C. Han, "Deep CNN-Based Spherical-Wave Channel Estimation for Terahertz Ultra-Massive MIMO Systems," in *GLOBECOM 2020 - 2020 IEEE Global Communications Conference*. IEEE, Dec. 2020, pp. 1–6.
- [30] K. Dovelos, M. Matthaiou, H. Q. Ngo, and B. Bellalta, "Channel Estimation and Hybrid Combining for Wideband Terahertz Massive MIMO Systems," *IEEE J. Sel. Areas Commun.*, vol. 39, no. 6, pp. 1604–1620, Apr. 2021.
- [31] A. M. Elbir, W. Shi, K. V. Mishra, and S. Chatzinotas, "Federated Learning for THz Channel Estimation," *arXiv*, Jul. 2022.

- [32] Z. Sha and Z. Wang, "Channel Estimation and Equalization for Terahertz Receiver With RF Impairments," *IEEE J. Sel. Areas Commun.*, vol. 39, no. 6, pp. 1621–1635, Apr. 2021.
- [33] J. Gao, C. Zhong, G. Y. Li, J. B. Soriaga, and A. Behboodi, "Deep Learning-based Channel Estimation for Wideband Hybrid MmWave Massive MIMO," *arXiv*, May 2022.
- [34] M. Cui, L. Dai, R. Schober, and L. Hanzo, "Near-Field Wideband Beamforming for Extremely Large Antenna Arrays," *arXiv*, Sep. 2021.
- [35] A. M. Elbir and T. E. Tuncer, "2-D DOA and mutual coupling coefficient estimation for arbitrary array structures with single and multiple snapshots," *Digital Signal Process.*, vol. 54, pp. 75–86, Jul. 2016.
- [36] Z.-M. Liu, Z.-T. Huang, and Y.-Y. Zhou, "An Efficient Maximum Likelihood Method for Direction-of-Arrival Estimation via Sparse Bayesian Learning," *IEEE Trans. Wireless Commun.*, vol. 11, no. 10, pp. 1–11, Sep. 2012.
- [37] H. Tang, J. Wang, and L. He, "Off-Grid Sparse Bayesian Learning-Based Channel Estimation for MmWave Massive MIMO Uplink," *IEEE Wireless Commun. Lett.*, vol. 8, no. 1, pp. 45–48, Jun. 2018.
- [38] M. E. Tipping, "Sparse bayesian learning and the relevance vector machine," *Journal of machine learning research*, vol. 1, no. Jun, pp. 211–244, 2001.
- [39] A. P. Dempster, N. M. Laird, and D. B. Rubin, "Maximum Likelihood from Incomplete Data Via the EM Algorithm," *Journal of the Royal Statistical Society: Series B (Methodological)*, vol. 39, no. 1, pp. 1–22, Sep. 1977.
- [40] B. M. Radich and K. M. Buckley, "Single-snapshot DOA estimation and source number detection," *IEEE Signal Process. Lett.*, vol. 4, no. 4, pp. 109–111, Apr. 1997.
- [41] R. Schmidt, "Multiple emitter location and signal parameter estimation," *IEEE Trans. Antennas Propag.*, vol. 34, no. 3, pp. 276–280, 1986.
- [42] E. J. Candes and M. B. Wakin, "An Introduction To Compressive Sampling," *IEEE Signal Process. Mag.*, vol. 25, no. 2, pp. 21–30, Mar. 2008.
- [43] X. Tan and J. Li, "Compressed Sensing via Sparse Bayesian Learning and Gibbs Sampling," in *2009 IEEE 13th Digital Signal Processing Workshop and 5th IEEE Signal Processing Education Workshop*. IEEE, Jan. 2009, pp. 690–695.
- [44] Z.-M. Liu and Y.-Y. Zhou, "A Unified Framework and Sparse Bayesian Perspective for Direction-of-Arrival Estimation in the Presence of Array Imperfections," *IEEE Trans. Signal Process.*, vol. 61, no. 15, pp. 3786–3798, May 2013.
- [45] Y. Xing and T. S. Rappaport, "Propagation measurement system and approach at 140 GHz - Moving to 6G and above 100 GHz," in *IEEE Global Communications Conference*, 2018, pp. 1–6.
- [46] S. Ju and T. S. Rappaport, "140 GHz Urban Microcell Propagation Measurements for Spatial Consistency Modeling," in *ICC 2021 - IEEE International Conference on Communications*. IEEE, Jun. 2021, pp. 1–6.
- [47] K. M. S. Huq, S. A. Busari, J. Rodriguez, V. Frascolla, W. Bazzi, and D. C. Sicker, "Terahertz-Enabled Wireless System for Beyond-5G Ultra-Fast Networks: A Brief Survey," *IEEE Network*, vol. 33, no. 4, pp. 89–95, Jul 2019.
- [48] Y. Lu, M. Hao, and R. Mackenzie, "Reconfigurable intelligent surface based hybrid precoding for THz communications," *Intelligent and Converged Networks*, vol. 3, no. 1, pp. 103–118, 2022.
- [49] A. Alkhateeb and R. W. Heath, "Frequency selective hybrid precoding for limited feedback millimeter wave systems," *IEEE Trans. Commun.*, vol. 64, no. 5, pp. 1801–1818, 2016.
- [50] A. M. Elbir and T. E. Tuncer, "Far-field DOA estimation and near-field localization for multipath signals," *Radio Sci.*, vol. 49, no. 9, pp. 765–776, Sep. 2014.
- [51] A. M. Elbir, A. K. Papazafeiropoulos, and S. Chatzinotas, "Federated Learning for Physical Layer Design," *IEEE Commun. Mag.*, vol. 59, no. 11, pp. 81–87, Nov. 2021.
- [52] A. M. Elbir and S. Coleri, "Federated Learning for Channel Estimation in Conventional and RIS-Assisted Massive MIMO," *IEEE Trans. Wireless Commun.*, vol. 21, no. 6, pp. 4255–4268, Nov. 2021.
- [53] H. B. McMahan, E. Moore, D. Ramage, S. Hampson, and B. A. y. Arcas, "Communication-Efficient Learning of Deep Networks from Decentralized Data," *arXiv*, Feb 2016.
- [54] P. Stoica and A. Nehorai, "MUSIC, maximum likelihood, and Cramér-Rao bound: Further results and comparisons," *IEEE Transactions on Acoustics, Speech, and Signal Processing*, vol. 38, no. 12, pp. 2140–2150, 1990.